METEOROLOGICAL APPLICATIONS
Meteorol. Appl. **24**: 84–91 (2017)
Published online in Wiley Online Library
(wileyonlinelibrary.com) DOI: 10.1002/met.1607

RMetS
Royal Meteorological Society

Crop evapotranspiration assessment under climate change in the Pannonian basin during 1991–2050

Mărgărit-Mircea Nistor,[a]*† Sorin Cheval,[b] Alessandro F. Gualtieri,[a] Alexandru Dumitrescu,[c] Vanessa E. Boţan,[d] Alex Berni,[a] Gheorghe Hognogi,[e] Ioan A. Irimuş[f] and Cosmin G. Porumb-Ghiurco[g]

[a] *Department of Chemical and Geological Sciences, University of Modena and Reggio Emilia, Italy*
[b] *ICUB, Research Institute of the University of Bucharest, Romania*
[c] *National Meteorological Administration, Bucharest, Romania*
[d] *Department of Psychology, University of Sussex, Brighton, UK*
[e] *Department of Regional Geography and Territorial Planning, Faculty of Geography, Babeş-Bolyai University, Cluj-Napoca, Romania*
[f] *Department of Physical and Technical Geography, Faculty of Geography, Babeş-Bolyai University, Cluj-Napoca, Romania*
[g] *Human Geography and Tourism, Faculty of Geography, Babeş-Bolyai University, Cluj-Napoca, Romania*

ABSTRACT: The impact of climate on crop evapotranspiration (ET_c) was assessed in the Pannonian basin for the present (1991–2020) and future (2021–2050). Annual temperature, annual precipitation and monthly potential evapotranspiration are the main climate data used in the present study. The European land cover database was used for the spatial recognition of terrain vegetation of the countries which are found in the Pannonian basin. A difference of maximum annual temperature from 19.9 to 20.8 °C was observed in the investigated area between 1991–2020 and 2021–2050. Precipitation rates decrease from west (1800 mm) to east (below 400 mm), and the potential evapotranspiration varies from 500 to 800 mm. Four stages of crop growth were identified and for each stage the crop co-efficients were assessed. For present projections of climate data, the annual crop evapotranspiration variability is from 105 to 1087 mm and records the highest values in mid-season stage, over 630 mm. Future projections indicate that in the central and southern part of the Pannonian basin the annual crop evapotranspiration will increase. For both present and future projections, the lowest crop evapotranspiration was found in the cold season, because of lack of heat and lower values of the crop co-efficient.

KEY WORDS land cover; climate; seasonal evapotranspiration; crop co-efficient; Pannonian basin

Received 22 January 2016; Revised 4 April 2016; Accepted 18 June 2016

1. Introduction

Food resources and cultivated areas are one of the priorities of the development and sustainability agenda for humanity's future. Even if the globe is an endless source of food, the costs and good management of territories make a real difference between many agricultural regions of the world. In this scenario, the best areas are those that exhibit the most favourable conditions in terms of adequate climate for agriculture, morphological characteristics and fertile soils. Almost all agricultural lands and eco-regions need to preserve future functionality. Being a primary good that impacts society, agriculture and transportation, water represents the most valuable resource on a regional scale (Jiménez Cisneros *et al*., 2014). Hence, the quantity of available water is an important measure for recent climate change (Shahgedanova *et al*., 2005).

The present climate is warming (Shaver *et al*., 2000; Oerlemans, 2005; Dong *et al*., 2013; Xie *et al*., 2013) and, for the 21st Century, increases in average temperatures on one side and decreases in precipitation rates were announced (Stocks *et al*., 1998; IPCC, 2001; Stavig *et al*., 2005). Climate change is easily observed between different regions, e.g. the Alps range and Carpathians range, Pannonia plain and Po plain. In this work, climate data on precipitation, temperature and actual evapotranspiration together with Corine Land Cover 2006 are the main datasets that were taken into account. Boegh *et al.* (2009) created a model of water balance, considering the evapotranspiration and runoff modelling of main land cover types for Sjælland Island, Denmark.

Recently, Mojid *et al.* (2015) argued that climate change impacts the crop water demand. Prăvălie (2014) and IPCC (2007) recall that evapotranspiration on a global scale is related to the trend in temperature and other complex factors of an anthropogenic nature. As previously mentioned by Chen *et al.* (2006) and Kousari *et al.* (2013) reported that evapotranspiration is the third important climatic factor that controls terrestrial ecosystems and the atmosphere mass exchange. Thus, the assessment of crop evapotranspiration (ET_c) becomes a significant indicator that is commonly used in regional water balance and irrigation surveys. Kurnik *et al.* (2014), in their study of water deficit in agricultural regions of Europe, created a soil water balance model that included simulations of soil water deficit and actual evapotranspiration. The assessment of sensitive parameters using different evapotranspiration methods was attempted by Ambas and Baltas (2012) in the Prefecture of Florina, Western Macedonia. Nistor and Porumb-Ghiurco (2015) applied the geographical information system (GIS)

* Correspondence: M.-M. Nistor, Department of Chemical and Geological Sciences, University of Modena and Reggio Emilia, Via Campi 103, Modena, 41125, Italy. E-mail: renddel@yahoo.com

†Current affiliation: Nanyang Technological University, School of Civil and Environmental Engineering, 42 Nanyang Avenue, Singapore

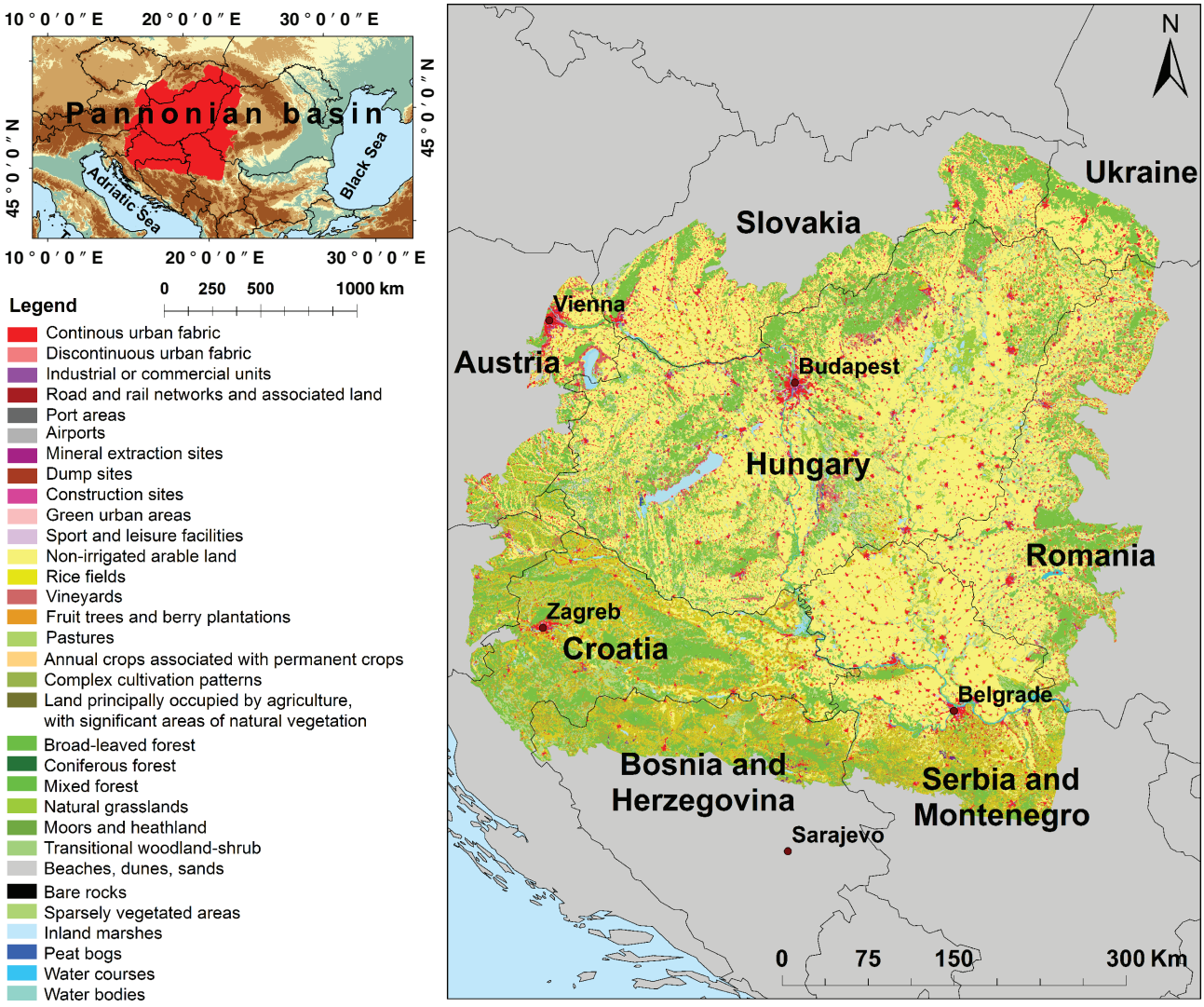

Figure 1. Location of the Pannonian basin on the Europe map (a) and land cover of the Pannonian basin (b).

applications and empirical formulae to calculate the land cover evapotranspiration on a regional scale. Recently, Nistor (2016) used GIS to compute the spatial distribution of climate indices in the Emilia-Romagna region. Thus, the present methodology was adopted from similar studies related to crop evapotranspiration (ET_c) in the Emilia-Romagna region (Nistor and Porumb-Ghiurco, 2015) and the Carpathian region of Europe (Nistor *et al.*, 2016).

In this study, the ET_c is assessed at the spatial level of the Pannonia basin under the present and future climate.

2. Study area

The Pannonian basin is located in the central part of Europe, between 43 ° 50′ and 49 ° 15′ latitude N and 15 ° 06′ and 23 ° 30′ longitude E (Figure 1). The region largely overlaps with the Pannonian plain and extends over nine countries: Austria, Slovenia, Hungary, Croatia, Bosnia-Herzegovina, Serbia and Montenegro, Romania, Slovakia and Ukraine. The physical characteristics of the Pannonian basin are the low land including the Great Hungarian Plain, the Danube plain, the Sava plain and the Drava plain (European Environment Agency, 2007). The surroundings of this region are bounded by the Alps range in the west, by the Carpathians in the north and east and by the Dinarics in the south.

As far as the climate is concerned, the Pannonian basin is characterized as fully humid Cfa in the southeastern part of the region and Cfb in most of the territory (Kottek *et al.*, 2006). The Cfb climate class is characterized by a fully humid climate with warm summers (Kottek *et al.*, 2006). The Pannonian basin has a Dfb climate near the Carpathian mountains in the northeastern side and on the western side close to the Alps. The Dfb climate class represents a humid continental climate, characterized by fully humid seasons with warm summers and cold winters (Kottek *et al.*, 2006). The precipitation ranges from 400 mm in the eastern part to 1800 mm in the western part. The highest annual temperature of the Pannonian basin is up to 12.64 °C in the south-central parts of the region and displays the lowest values in the northern part of the region. The potential evapotranspiration (ET_0) ranges from 586 to 739 mm. The average precipitation, temperature and ET_0 climate data relative to the recent period (1991–2020) and future period (2021–2050) are shown in Figure 2.

The main types of soils found in the study area are chernozems and black soils rich in humus (European Environment Agency, 2007), characterizing the Pannonian basin as an important agricultural land in central Europe. The widespread land cover area

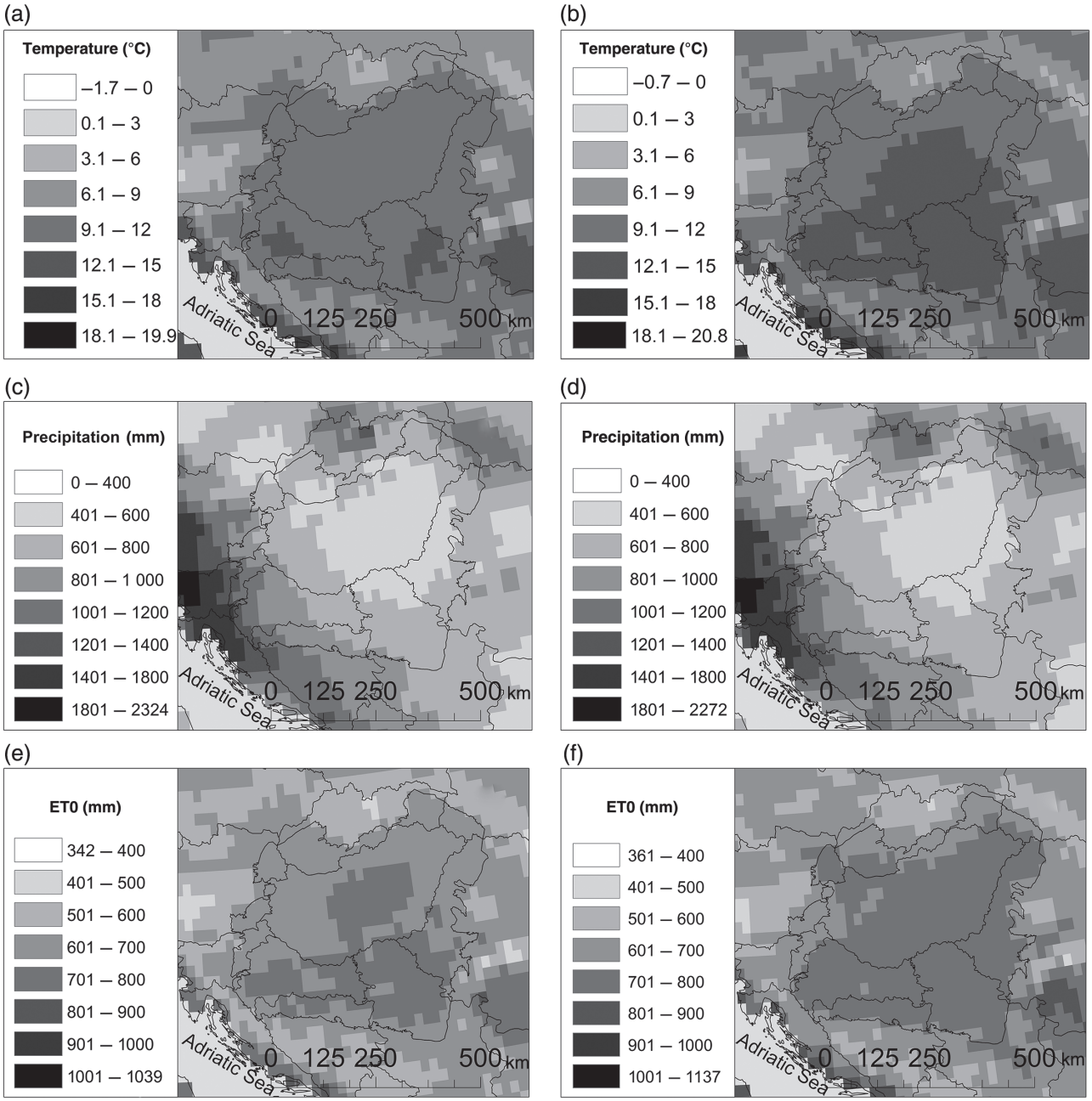

Figure 2. (a) The mean annual air temperature between 1991 and 2020. (b) The average of the mean annual air temperature between 2021 and 2050. (c) The average of the mean annual precipitation between 1991 and 2020. (d) The average of the mean annual precipitation between 2021 and 2050. (e) The average annual ET_0 between 1991 and 2020. (f) The average annual ET_0 between 2021 and 2050.

is represented by grass, pasture, agricultural area and forest. The forest land includes the main species of oak (*Quercus*), beech (*Fagus*), elm (*Ulmus*) and hornbeam (*Carpinus)* (European Environment Agency, 2007).

3. Materials and methods

3.1. Climate and land cover data

Raster data grids of $25 \times 25\,km^2$ for the precipitation, temperature and ET_0 data were used in the present study. These maps represent the space distribution of the above parameters calculated as average values within a time span of 30 years. The models were carried out in the framework of the CC-WARE European project by the National Meteorological Administration from Bucharest and cover southeast Europe (Čenčur Curk *et al.*, 2014). For the present time the average climate data from 1991 to 2020 were used and for the future projection the average climate data from 2021 to 2050 were used. These climate datasets were obtained using the RegCM3, ALADIN and PROMES models considering the A1B scenario proposed by IPCC (2001). The A1B scenario assumes economic growth, population increase and expert technology up to the mid 21st Century.

The land cover information used here belongs to the Corine Land Cover database, dating to 2006. The land cover is divided into five classes, each one detailed up to the fourth level of land type categories. The details given by the Corine Land

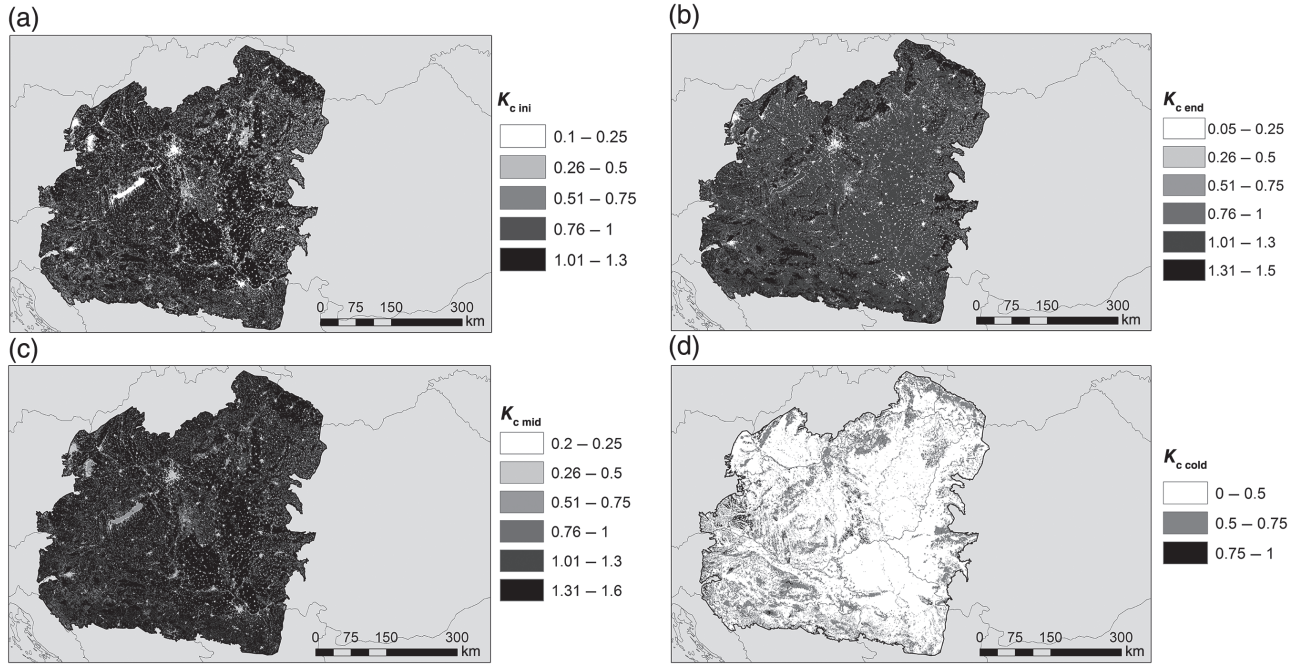

Figure 3. Spatial distribution of K_c in the Pannonian basin. (a) $K_{c\ ini}$ for the initial stage, (b) $K_{c\ mid}$ for the mid-season stage, (c) $K_{c\ end}$ for the late stage and (d) $K_{c\ cold}$ for the cold stage.

Cover database justify their contribution to this study. In the northeastern extremity, in the Ukraine territory, Global Land Cover was used because Corine Land Cover does not cover this area. The Global Land Cover was elaborated by China in collaboration with the United Nations and contains 10 classes, which were attached to the Corine Land Cover.

3.2. Potential evapotranspiration data (ET_0)

Monthly ET_0 data grids of southeast Europe were used in the calculation of the seasonal and annual ET_c. ET_0 was calculated using the Thornthwaite (1948) formula (Equation (1)). The Thornthwaite method has been used in several studies (Čenčur Curk *et al.*, 2014; Nistor *et al.*, 2015):

$$ET_0 = 16\frac{L}{12}\frac{N}{30}\left(\frac{10T_i}{I}\right)^{\alpha} \quad (1)$$

where ET_0 is the monthly potential evapotranspiration (mm), L is the average day length of the month being calculated (h), N is the number of days in the month being calculated, T_i is the average monthly temperature (°C), $ET_0 = 0$ if $T_i < 0$, I is the heat index (Equation (2)) and α is a complex function of the heat index (Equation (3)):

$$I = \sum_{i=1}^{12}\left(\frac{T_i}{5}\right)^{1.514} \quad (2)$$

where T_i is the monthly air temperature:

$$\alpha = 6.75 \times 10^{-7} I^3 - 7.71 \times 10^{-5} I^2 + 1.7912 \times 10^{-2} I + 0.49239 \quad (3)$$

where I is the annual heat index.

The present period (1991–2020) and future period (2021–2050) data grids of ET_0 were computed on the basis of temperature data obtained through the RegCM3, ALADIN and PROMES models. The models were constructed according to the A1B scenario (IPCC, 2001).

3.3. Crop co-efficient (K_c)

A specific value of the crop co-efficient (K_c) for each land cover type was assigned in order to calculate the crop evapotranspiration ET_c. The K_c used for the calculations of ET_c may vary slightly from one study case to another depending on the local conditions. Here, the method of a standard single K_c presented in the report of the Food and Agriculture Organization was adopted (Allen *et al.*, 1998). Regarding crop growth, K_c takes different values (Allen *et al.*, 1998; Grimmond and Oke, 1999; Nistor and Porumb-Ghiurco, 2015; Nistor *et al.*, 2016). The method proposed by Nistor and Porumb-Ghiurco (2015) and Nistor *et al.* (2016) regarding regional ET_c shows four seasons of crop growth during 1 year: initial, mid-season, late season and cold season. In this study, the same methodology based on four seasons of crop growth was chosen. Between initial and mid-season a development stage occurs, but from overlap of the crop growth periods it is assumed that this stage could easily be included in the initial season (Nistor and Porumb-Ghiurco, 2015; Nistor *et al.*, 2016). Thus, a specific K_c was used for the initial season ($K_{c\ ini}$), a specific K_c was used for mid-season ($K_{c\ mid}$), a specific K_c was used for late season ($K_{c\ end}$) and $K_{c\ cold}$ was used for the cold season. The evapotranspiration rates from urban areas and bare soil were published by Grimmond and Oke (1999). They use K_c values related to different places in the United States. Based on their study, the values of K_c related to urban areas and bare soil were chosen considering the latitude as a factor of relevance. Figure 3 depicts the spatial distribution of K_c in the Pannonian basin. Table 1 reports the K_c values used in the present study.

3.4. Crop evapotranspiration (ET_c)

The annual ET_c of the Pannonian basin was calculated by summing the four seasons of ET_c (Equation (4)). First, the initial ET_c ($ET_{c\ ini}$) (Equation (5)), the mid-season ET_c ($ET_{c\ mid}$) (Equation (6)), the late season ET_c ($ET_{c\ end}$) (Equation (7)) and

Table 1. Corine Land Cover co-efficients used for seasonal ET_c in the Pannonian basin.

Corine Land Cover		K_c initial season					K_c mid season					K_c end season					K_c cold season				
CLC code 2006	CLC description	Kc	Ks	Ku	Kw	Kclc	Kc	Ks	Ku	Kw	Kclc	Kc	Ks	Ku	Kw	Kclc	Kc	Ks	Ku	Kw	Kclc
111	Continuous urban fabric	–	–	0.2	–	0.2	–	–	0.4	–	0.4	–	–	0.25	–	0.25	–	–	–	–	–
112	Discontinuous urban fabric	–	–	0.1	–	0.1	–	–	0.3	–	0.3	–	–	0.2	–	0.2	–	–	–	–	–
121	Industrial or commercial units	–	–	0.2	–	0.2	–	–	0.4	–	0.4	–	–	0.3	–	0.3	–	–	–	–	–
122	Road and rail networks and associated land	–	–	0.15	–	0.15	–	–	0.35	–	0.35	–	–	0.25	–	0.25	–	–	–	–	–
123	Port areas	–	–	0.3	–	0.3	–	–	0.5	–	0.5	–	–	0.4	–	0.4	–	–	–	–	–
124	Airports	–	–	0.2	–	0.2	–	–	0.4	–	0.4	–	–	0.3	–	0.3	–	–	–	–	–
131	Mineral extraction sites	–	–	0.16	–	0.16	–	–	0.36	–	0.36	–	–	0.26	–	0.26	–	–	–	–	–
132	Dump sites	–	–	0.16	–	0.16	–	–	0.36	–	0.36	–	–	0.26	–	0.26	–	–	–	–	–
133	Construction sites	–	–	0.16	–	0.16	–	–	0.36	–	0.36	–	–	0.26	–	0.26	–	–	–	–	–
141	Green urban areas	–	–	0.12	–	0.12	–	–	0.32	–	0.32	–	–	0.22	–	0.22	–	–	–	–	–
142	Sport and leisure facilities	–	–	0.1	–	0.1	–	–	0.3	–	0.3	–	–	0.2	–	0.2	–	–	–	–	–
211	Non-irrigated arable land	1.1	–	–	–	1.1	1.35	–	–	–	1.35	1.25	–	–	–	1.25	–	–	–	–	–
213	Rice fields	1.05	–	–	–	1.05	1.2	–	–	–	1.2	0.6	–	–	–	0.6	–	–	–	–	–
221	Vineyards	0.3	–	–	–	0.3	0.7	–	–	–	0.7	0.45	–	–	–	0.45	–	–	–	–	–
222	Fruit trees and berry plantations	0.3	–	–	–	0.3	1.05	–	–	–	1.05	0.5	–	–	–	0.5	–	–	–	–	–
231	Pastures	0.4	–	–	–	0.4	0.9	–	–	–	0.9	0.8	–	–	–	0.8	–	–	–	–	–
241	Annual crops associated with permanent crops	0.5	–	–	–	0.5	0.8	–	–	–	0.8	0.7	–	–	–	0.7	–	–	–	–	–
242	Complex cultivation patterns	1.1	–	–	–	1.1	1.35	–	–	–	1.35	1.25	–	–	–	1.25	–	–	–	–	–
243	Land principally occupied by agriculture, with significant areas of natural vegetation	0.7	–	–	–	0.7	1.15	–	–	–	1.15	1	–	–	–	1	–	–	–	–	–
311	Broad-leaved forest	1.3	–	–	–	1.3	1.6	–	–	–	1.6	1.5	–	–	–	1.5	0.6	–	–	–	0.6
312	Coniferous forest	1	–	–	–	1	1	–	–	–	1	1	–	–	–	1	1	–	–	–	1
313	Mixed forest	1.2	–	–	–	1.2	1.5	–	–	–	1.5	1.3	–	–	–	1.3	0.8	–	–	–	0.8
321	Natural grasslands	0.3	–	–	–	0.3	1.15	–	–	–	1.15	1.1	–	–	–	1.1	–	–	–	–	–
322	Moors and heathland	0.8	–	–	–	0.8	1	–	–	–	1	0.95	–	–	–	0.95	–	–	–	–	–
324	Transitional woodland–shrub	0.8	–	–	–	0.8	1	–	–	–	1	0.95	–	–	–	0.95	–	–	–	–	–
331	Beaches, dunes, sands	–	0.2	–	–	0.2	-	0.3	–	–	0.3	–	0.25	–	–	0.25	–	–	–	–	–
332	Bare rocks	–	0.15	–	–	0.15	–	0.2	–	–	0.2	–	0.05	–	–	0.05	–	–	–	–	–
333	Sparsely vegetated areas	0.4	–	–	–	0.4	0.6	–	–	–	0.6	0.5	–	–	–	0.5	–	–	–	–	–
411	Inland marshes	–	–	–	0.15	0.15	–	–	–	0.45	0.45	–	–	–	0.8	0.8	–	–	–	–	–
412	Peat bogs	–	–	–	0.1	0.1	–	–	–	0.4	0.4	–	–	–	0.75	0.75	–	–	–	–	–
511	Water courses	–	–	–	0.25	0.25	–	–	–	0.65	0.65	–	–	–	1.25	1.25	–	–	–	–	–
512	Water bodies	–	–	–	0.25	0.25	–	–	–	0.65	0.65	–	–	–	1.25	1.25	–	–	–	–	–

Kc, crop co-efficient for plants; Ks, evaporation co-efficient for bare soils; Ku, crop co-efficient for urban areas; Kw, evaporation co-efficient for open water; Kclc, crop co-efficient for land cover.
Source: From Allen *et al.* (1998) and Nistor and Porumb-Ghiurco (2015).

the cold ET_c ($ET_{c\,cold}$) (Equation (8)) were calculated, multiplying the ET_0 of each set season by the seasonal value of K_c. The seasonal ET_c and annual ET_c were calculated using ArcGIS from an ESRI environment. The software was capable of providing mathematical calculations between raster data and has been successfully used on climate data processing and spatial data analysis by Baltas (2007), Nistor (2014a, 2014b), Dezsi *et al.* (2015), Nistor and Petcu (2015), Nistor and Porumb (2015), Nistor *et al.* (2015). The mathematical calculations of seasonal ET_c and annual ET_c were done using the 'Raster Calculator' function from the 'Map Algebra' tool which is able to execute the raster data operations between different layers:

$$\text{annual } ET_c = ET_{c\,ini} + ET_{c\,mid} + ET_{c\,end} + ET_{c\,cold} \quad (4)$$

$$ET_{c\,ini} = ET_{0\,ini} \times K_{c\,ini} \quad (5)$$

$$ET_{c\,mid} = ET_{0\,mid} \times K_{c\,mid} \quad (6)$$

$$ET_{c\,end} = ET_{0\,end} \times K_{c\,end} \quad (7)$$

$$ET_{c\,cold} = ET_{0\,cold} \times K_{c\,cold} \quad (8)$$

4. Results

Figure 4 depicts the seasonal ET_c spatial distribution of the Pannonian basin for the present and future time. During the initial season, the $ET_{c\,ini}$ values range from 13 to 236 mm in the present period and from 14 to 240 mm in the future period. Due to the impact of climate changes, an increase of ET_{ini} between present and future was observed, especially during the spring months (March–May).

The $ET_{c\,mid}$ shows values between 74 and 635 mm in the present period and values between 79 and 680 mm in the future period. The maximum values of $ET_{c\,mid}$ in the present period display a limited spread in the centre, north and southwestern part of the Pannonian basin and in some locations of the eastern part,

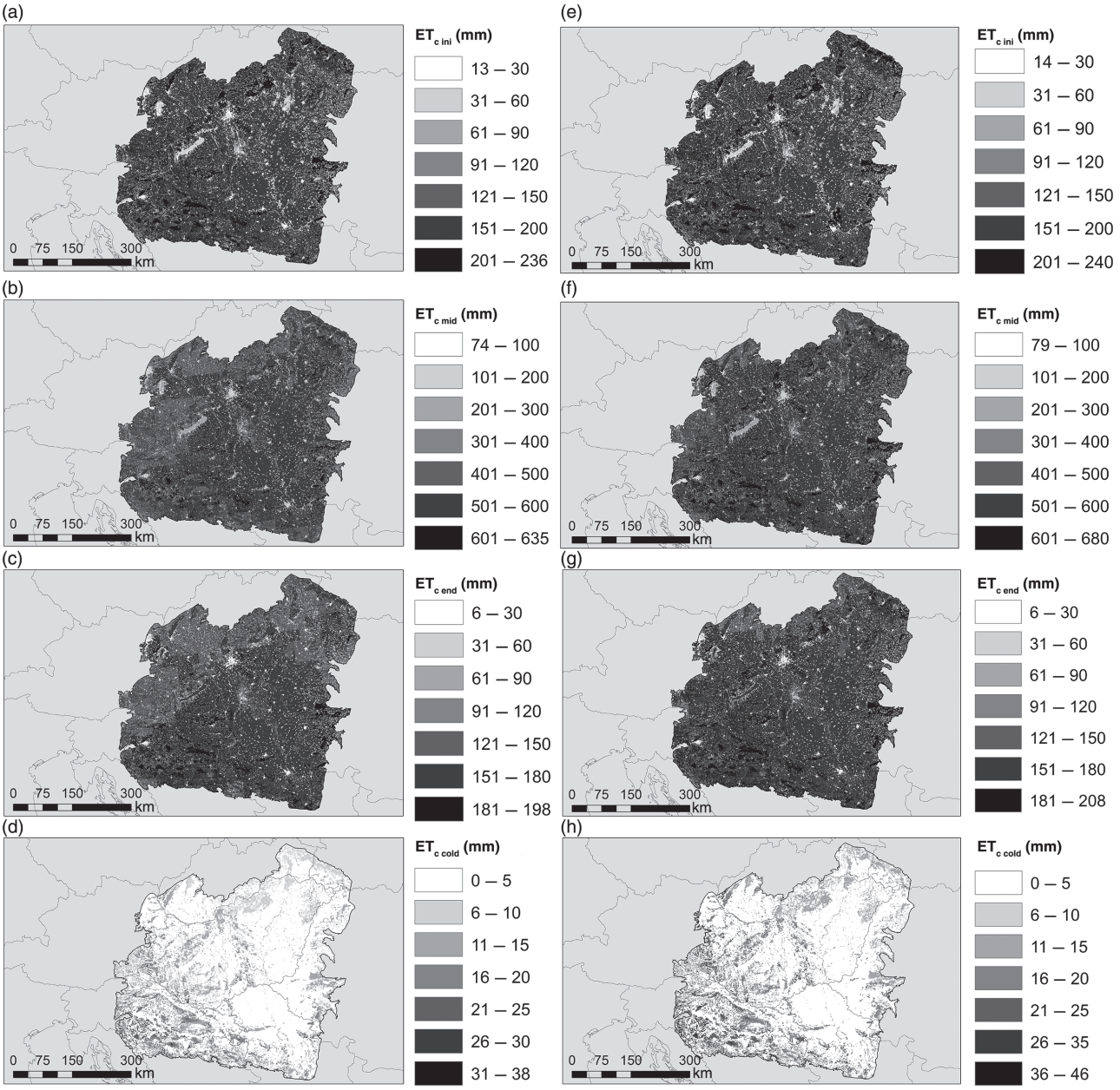

Figure 4. Spatial distribution of seasonal ET_c in the Pannonian basin. (a) $ET_{c\ ini}$ for the initial stage (1991–2020). (b) $ET_{c\ mid}$ for the mid-season stage (1991–2020). (c) $ET_{c\ end}$ for the late stage (1991–2020). (d) $ET_{c\ cold}$ for the cold stage (1991–2020). (e) $ET_{c\ ini}$ for the initial stage (2021–2050). (f) $ET_{c\ mid}$ for the mid-season stage (2021–2050). (g) $ET_{c\ end}$ for the late stage (2021–2050). (h) $ET_{c\ cold}$ for the cold stage (2021–2050).

near the border of Hungary with Romania. In the future period the maximum values of $ET_{c\ mid}$ spread over southern, northern and western sides of the region, especially in the east of Croatia and north of Bosnia and Herzegovina. High values of $ET_{c\ mid}$ were also found in the east sides of the region, in correspondence with the Hungarian territory. The maximum values of $ET_{c\ mid}$ correspond to land covered by broad leaved and mixed forests. The areas with the lowest $ET_{c\ mid}$ values are located in the west, southeastern and northwestern parts of the region. These areas overlap inland marshes and open water lands, where the ET_0 values are below 700 mm year^{-1}.

The $ET_{c\ end}$ ranges from 6 to 198 mm in the present period and from 6 to 208 mm in the future period. Focusing on the end seasons, during 1991–2020 $ET_{c\ end}$ displays high values of 150–198 mm in the southwestern part of the region and in a few locations of the central and eastern sides of the Pannonian basin. In the 2021–2050 period, $ET_{c\ end}$ reaches maximum values of more than 200 mm in the southwestern, western and eastern sides of the Pannonian basin. In the northwestern part, high values of $ET_{c\ end}$ are found for the future period. The minimum values of $ET_{c\ end}$ fall below 10 mm in both periods. No significant differences are detected in the space distribution of $ET_{c\ end}$, because the pattern of land cover is the same and no strong climate changes are found in the autumn.

The cold season shows values from 0 to 38 mm for $ET_{c\ cold}$ in the present and values from 0 to 46 mm in the future period. The low values of $ET_{c\ cold}$ are influenced by the lower temperature in the cold season. The maximum values of both analysed periods could be found in the area covered by coniferous forest. Strong changes of $ET_{c\ cold}$ are calculated in the southwestern part of the

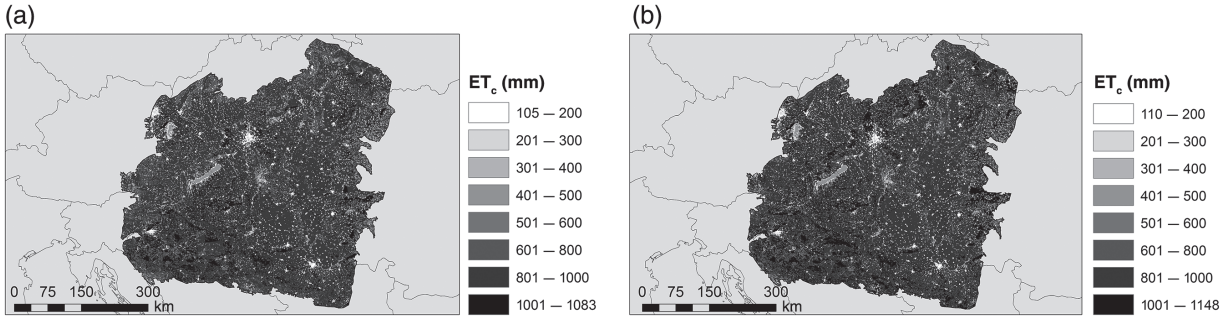

Figure 5. Spatial distribution of annual ET_c in the Pannonian basin. (a) Annual ET_c for the present period (1991–2020). (b) Annual ET_c for the future period (2021–2050).

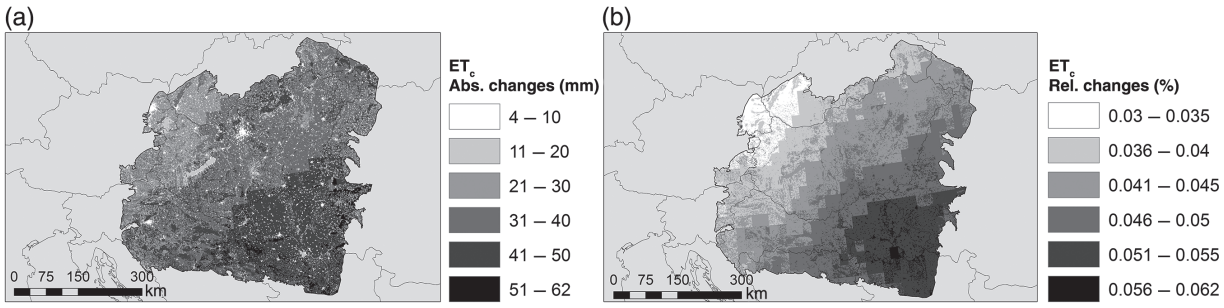

Figure 6. (a) Absolute changes of annual ET_c in the Pannonian basin between the future and present periods. (b) Relative changes of annual ET_c in the Pannonian basin between the future and present periods.

Pannonian basin between present and future. These areas refer to the north of Croatia, the north of Serbia and the north of Bosnia and Herzegovina. No significant changes of $ET_{c\ cold}$ at the edges of Austria, Slovakia, Hungary and Romania included in the Pannonian region were highlighted. In the Ukraine, $ET_{c\ cold}$ increases between present and future by 6–15 mm. The land cover pattern denotes that the $K_{c\ cold}$ values of forest contribute an increase of $ET_{c\ cold}$ even if the temperatures fall below 5 °C in November–February.

The present and future annual ET_c distributions are shown in Figure 5. As expected, the annual ET_c has highest values in the southern part, where the temperatures are higher than 12 °C. The maximum value of annual ET_c in the present scenario is 1083 mm. High values are found in south and central Hungary, north of Croatia and west Romania. The future scenario shows maximum values of annual ET_c up to 1148 mm. The high values of annual ET_c in the present and future are attributed to the high values of temperature and to the forest and cultivated lands with the highest K_c. The space distributions of annual ET_c in both set periods are also influenced by temperatures over 12 °C in the south and central part of the region. The sides with maximum values of annual ET_c show land cover patterns with a mixed type of forest, and this explains why high values of K_c contribute to the rise in annual ET_c. The lowest values of annual ET_c are found in the northwestern part of the Pannonian basin, in some locations of the Ukraine territory and generally in the extended urban areas (e.g. Budapest) due to lower K_c values during the year for both periods, present and future.

The absolute and relative changes between present and future are illustrated in Figure 6. To observe the most affected areas and the areas with fewer changes in annual ET_c the absolute and relative changes between future and present were assessed. The highest values of absolute changes (62 mm) are in the central and southeastern part, in the south of Hungary, west of Romania and north of Serbia. The low values of absolute changes are located in the west, north and northeastern parts of the Pannonian basin, in the territories of Austria, Hungary, Slovakia and Ukraine. The relative changes have high values (0.062%) in southeastern part of the Pannonian region, especially in northern Serbia.

5. Conclusions

The main aim of the study was to calculate crop evapotranspiration ((ET_c) in the Pannonian basin for the present and future periods. Even if the goals were achieved, limitations come from overlapping growth of each land cover type. The complex cultivation period data of the Pannonian basin is hard to integrate in four stages, because the real situation requires more overlaps between crop growth. Nistor and Porumb (2015) explain very well how to evaluate the ET_c at regional level, applying the same methodology to the data relative to the Emilia-Romagna region in Italy.

The work presented here shows how to assess the ET_c at space level using the land cover database and climatological spatial data. The methods should be improved with specific field measurements, to be closer to the real situation. Climate changes mostly contribute in the distribution of evapotranspiration in the Pannonian basin. The work applies well to management and assessment of water resources in agricultural lands. The future scenario shows how ET_c in the Pannonian basin will evolve under the climate change during 2021–2050. Several places from the south and southwestern sides of the region with values of annual ET_c exceeding 1000 mm were found. The findings are useful to agriculture planning, climatology of the Pannonian basin and for identification of critical water areas and irrigation demand areas. In the future, the focus will be on the projection of land cover, not only on scenarios related to climate data. The results may be

useful in the calculation of groundwater vulnerability of the area under climate change.

Acknowledgements

The authors would like to thank to the European Environment Agency which provided the land cover data for the whole Europe.

References

Allen RG, Pereira LS, Raes D, Smith M. 1998. *Crop Evapotranspiration: Guidelines for Computing Crop Water Requirements*. FAO Irrigation and Drainage Paper 56. FAO: Rome; 300 pp.

Ambas VT, Baltas E. 2012. Sensitivity analysis of different evapotranspiration methods using a new sensitivity coefficient. *Global Nest J.* **14**(3): 335–343.

Baltas E. 2007. Spatial distribution of climatic indices in northern Greece. *Meteorol. Appl.* **14**: 69–78.

Boegh E, Poulsen RN, Butts M, Abrahamsen P, Dellwik E, Hansen S, et al. 2009. Remote sensing based evapotranspiration and runoff modeling of agricultural, forest and urban flux sites in Denmark: from field to macro-scale. *J. Hydrol.* **377**: 300–316.

Čenčur Curk B, Cheval S, Marjanović P, Siegel H, Gerhardt E, Hochbichler E *et al.* 2014. CC-WARE mitigating vulnerability of water resources under climate change, WP3 – vulnerability of water resources in SEE, report version 5. http://www.ccware.eu/output-documentation/output-wp3.html (accessed 20 November 2015).

Chen SB, Liu YF, Thomas A. 2006. Climatic change on the Tibetan plateau: potential evapotranspiration trends from 1961 to 2000. *Clim. Change* **76**: 291–319.

Dezsi Ş, Nistor MM, Man TC, Rusu R. 2015. The GIS assessment of a winter sports resort location. Case study: Beliş District, Western Carpathians. *Carpathian J. Earth Environ. Sci.* **10**(1): 223–230.

Dong P, Wang C, Ding J. 2013. Estimating glacier volume loss used remotely sensed images, digital elevation data, and GIS modelling. *Int. J. Remote Sens.* **34**(24): 8881–8892.

European Environment Agency. 2007. *The Pannonian Region – The Remains of the Pannonian Sea*, Condé S, Richard D, Liamine N, Leclère AS, Sotolargo B, Pinborg U (eds). ZooBoTech HB Ed.: Lund, Sweden.

Grimmond CSB, Oke TR 1999. Evapotranspiration rates in urban areas, Impacts of Urban Growth on Surface Water and Groundwater Quality. *Proceedings of IUGG 99 Symposium HSS*. Birmingham, July J999, IAHS Publ. no. 259; 235–243.

IPCC. 2001. Climate change 2001: the scientific basis. In *Contribution of Working Group I to the Third Assessment Report of the Intergovernmental Panel on Climate Change*, Houghton JT, Ding Y, Griggs DJ, Noguer M, van der Linden PJ, Dai X, Maskell K, Johnson CA (eds). Cambridge University Press: Cambridge and New York, NY; 881 pp.

IPCC. 2007. *Climate Change 2007: Impacts, Adaptation and Vulnerability. Contribution of Working Group II to the Fourth Assessment Report of the Intergovernmental Panel on Climate Change*, Parry ML, Canziani OF, Palutikof JP, van der Linden PJ, Hanson CE (eds). Cambridge University Press: Cambridge; 976.

Jiménez Cisneros BE, Oki T, Arnell NW, Benito G, Cogley JG, Döll P, et al. 2014. Freshwater resources. In *Climate Change 2014: Impacts, Adaptation, and Vulnerability. Part A: Global and Sectoral Aspects. Contribution of Working Group II to the Fifth Assessment Report of the Intergovernmental Panel on Climate Change*, Field CB, Barros VR, Dokken DJ, Mach KJ, Mastrandrea MD, Bilir TE, Chatterjee M, Ebi KL, Estrada YO, Genova RC, Girma B, Kissel ES, Levy AN, MacCracken S, Mastrandrea PR, White LL (eds). Cambridge University Press: Cambridge; 229–269.

Kottek M, Grieser J, Beck C, Rudolf B, Rubel F. 2006. World map of the Köppen–Geiger climate classification updated. *Meteorol. Z.* **15**(3): 259–263.

Kousari MR, Zarch MAA, Ahani H, Hakimelahi H. 2013. A survey of temporal and spatial reference crop evapotranspiration trends in Iran from 1960 to 2005. *Clim. Change* **120**: 277–298.

Kurnik B, Kajfež-Bogataj L, Horionc S. 2014. An assessment of actual evapotranspiration and soil water deficit in agricultural regions in Europe. *Int. J. Climatol.* **35**(9): 2451–2471, DOI: 10.1002/joc.4154.

Mojid MA, Rannu RP, Karim NN. 2015. Climate change impacts on reference crop evapotranspiration in North-West hydrological region of Bangladesh. *Int. J. Climatol.* **35**(13): 4041–4046, DOI: 10.1002/joc.4260.

Nistor MM. 2014a. Using Landsat images and GIS to assess the changes of Mer de Glace and Marmolada Glaciers, in the last three decades. *Stud. UBB Geogr.* **LIX**(1): 65–76.

Nistor MM. 2014b. *Using GIS Techniques for the Projection of Ski Tracks in Western Carpathians. Case Study: Beliş District*. Cluj University Press: Cluj-Napoca. e-book, ISBN 978-973-595-709-4. http://www.editura.ubbcluj.ro/www/ro/ebooks/authors_d.php?ida=1068 (accessed 5 December 2015) (in Romanian).

Nistor MM. 2016. Spatial distribution of climate indices in Emilia-Romagna region. *Meteorol. Appl.* **23**: 304–313, DOI: 10.1002/met.1555.

Nistor MM, Dezsi , Cheval S. 2015. Vulnerability of groundwater under climate change and land cover: a new spatial assessment method applied on Beliş district (Western Carpathians, Romania). *Environ. Eng. Manage. J.* **14**(12): 2959–2971.

Nistor MM, Gualtieri A, Cheval S, Dezsi Ş, Boţan VE. 2016. Climate change effects on crop evapotranspiration in the Carpathian Region during 1961-2010. *Meteorol. Appl.* **23**: 462–469.

Nistor MM, Petcu IM. 2015. Quantitative analysis of glaciers changes from Passage Canal based on GIS and satellite images, South Alaska. *Appl. Ecol. Environ. Res.* **13**(2): 535–549.

Nistor MM, Porumb-Ghiurco GC. 2015. How to compute the land cover evapotranspiration at regional scale? A spatial approach of Emilia-Romagna region. *GEOREVIEW Sci. Ann. Ştefan cel Mare Uni. Suceava Geogr. Ser.* **25**(1): 38–54.

Oerlemans J. 2005. Extracting a climate signal from 169 glacier records. *Science* **308**: 675–677.

Prăvălie R. 2014. Analysis of temperature, precipitation and potential evapotranspiration trends in southern Oltenia in the context of climate change. *Geogr. Tech.* **9**(2): 68–84.

Shahgedanova M, Stokes CR, Gurney SD, Popovnin V. 2005. Interactions between mass balance, atmospheric circulation, and recent climate change on the Djankuat Glacier, Caucasus Mountains, Russia. *J. Geophys. Res.* **110**(D4): 1–12.

Shaver GR, Canadell J, Chapin FS III, Gurevitch J, Harte J, Henry G, et al. 2000. Global warming and terrestrial ecosystems: a conceptual framework for analysis. *BioScience* **50**(10): 871–882.

Stavig L, Collins L, Hager C, Herring M, Brown E, Locklar E. 2005. The effects of climate change on Cordova, Alaska on the Prince William Sound. *Alaska Tsunami Papers.* Publishing Web. https://seagrant.uaf.edu/nosb/papers/2005/cordova-nurds.html (accessed 23 April 2014).

Stocks BJ, Fosberg MA, Lynham TJ, Mearns L, Wotton BM, Yang Q, et al. 1998. Climate change and forest fire potential in Russian and Canadian boreal forests. *Clim. Change* **38**: 1–13.

Thornthwaite CW. 1948. An approach toward a rational classification of climate. *Geogr. Rev.* **38**: 55–94.

Xie X, Li YX, Li R, Zhang Y, Huo Y, Bao Y, et al. 2013. Hyperspectral characteristics and growth monitoring of rice (Oryza sativa) under asymmetric warming. *Int. J. Remote Sens.* **34**(23): 8449–8462.

